JMES The International Journal of Mechanical Engineering and Sciences
https://journal.its.ac.id/index.php/jmes/index
e-ISSN 2580-7471

Incorporating Semiautomatic Coprecipitation Apparatus and Gas Nitriding for Synthesis of Iron Nitride from Natural Iron Sand

Indra Sidharta[1*], Intan Y. P. Perindasari[2], Darminto[2], Abdullah Shahab[1]

[1]Department of Mechanical Engineering, Institut Teknologi Sepuluh Nopember, Surabaya 60111, Indonesia
[2]Department of Physics, Institut Teknologi Sepuluh Nopember, Surabaya 60111, Indonesia

Received: 18 June 2026, Revised: 20 July 2026, Accepted: 22 July 2026

Abstract

This study aimed to synthesize iron nitride (Fe_3N) material using Fe_3O_4 as the starting material. The synthesis process included coprecipitation of natural iron sand and gas nitriding under flowing NH_3 gas. A semiautomatic coprecipitation apparatus was implemented during the coprecipitation process to improve powder yield and reproducibility of Fe_3O_4 nanopowders. The results of XRD and SEM showed that the semiautomatic coprecipitation apparatus could produce a consistent Fe_3O_4 product in terms of final quantity and powder morphology. Furthermore, Fe_3N was produced after gas nitriding for different holding times. Iron oxides, Fe_3O_4 and Fe_2O_3, were still detected in the powder, showing that the nitriding parameters were insufficient to produce Fe_3N completely. VSM measurement on the final powder showed typical soft magnetic behavior, with a maximum saturation magnetization of 17.21 emu/g and coercivity of 0.04 Oe after 6 hours of nitriding. This study provided an alternative method for local soft magnetic composite production using abundant Indonesian natural resources.

Keywords: iron nitride, Fe_3O_4, iron oxide, semiautomatic coprecipitation apparatus, gas nitriding, soft magnet.

1. Introduction

Iron nitride (Fe_3N) is a promising material for magnetic applications, due to its high saturation magnetization, low coercivity, and elevated resistivity [1–5]. Furthermore, Fe_3N exists in several phases, namely Fe_2N, Fe_3N, Fe_4N, Fe_8N, and Fe_6N_{12}, depending on the synthesis methods and nitrogen potential used during the process [6]. Fe_3N has prominent characteristics of soft magnets, serving as a potential alternative material for Soft Magnetic Composite (SMC) in electric vehicle (EV) applications. SMC is commonly produced using iron powder as the starter material [7–10]. Due to the absence of an iron powder industry, SMC development in Indonesia is highly dependent on imported materials.

The absence of iron powder presents an unfavorable obstacle to Indonesia's effort to transition transportation technology from internal combustion engines to EVs. Therefore, the development of alternative materials for SMC is essential. A recent report by Sidharta et al. [11] indicates that iron nitride can be synthesized from iron oxide powder derived from natural iron sand, which is abundantly found in the country [12–16]. Many efforts have been performed to produce iron oxide powder from natural sand, for magnetic applications [14, 17–20]. The iron oxide powder, preferably on the nanometer scale, is produced using numerous methods [21, 22].

Coprecipitation is the most commonly used method for synthesizing iron oxide nanopowder [21,23]. However, a number of limiting factors have been profoundly impeding the implementation of larger production capacity, such as a small quantity of the final product and quality stability in terms of powder size. To address these limitations, efforts have been instigated to scale up the coprecipitation process for industrial applications [23–25]. Only limited studies have achieved good results, i.e. high production capacity up to 23 kg/day and homogeneous size of iron oxide nanoparticles, in the scale-up of iron oxide nanopowder synthesis [25, 26]. Therefore, this study aimed to develop a scalable synthesis route for Fe_3N soft magnetic material using locally abundant iron sand through a semiautomatic coprecipitation and gas nitriding process.

2. Experimental method

This study used natural iron sand as the raw material for Fe_3N synthesis. The sand was obtained from a local Indonesian market. The synthesis process started with the magnetic separation of raw sand, followed by the removal of non-magnetic constituents. Subsequently, a coprecipitation process was carried out to obtain iron oxide nanopowder based on the procedures of Sunaryono et al. [27]. A total of two batches of iron sand samples, each weighing 12 g, were used in this study. A semiautomatic

*Corresponding author. Email: sidarta@me.its.ac.id

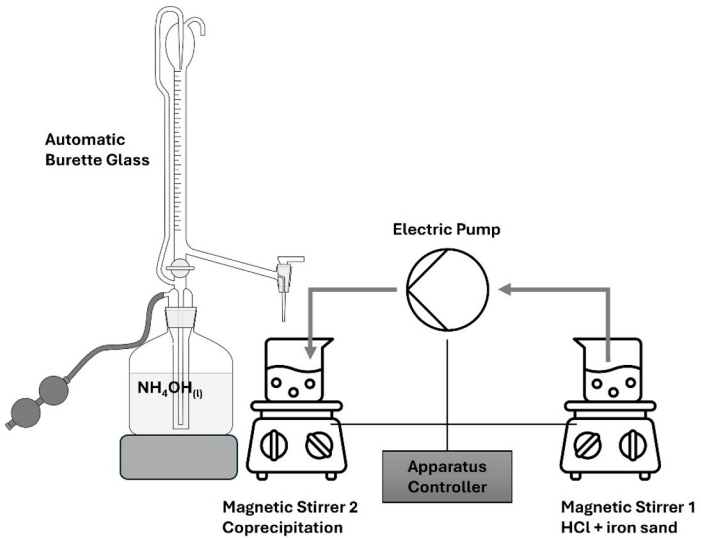

Figure 1. Schematic of semiautomatic coprecipitation apparatus. The image of automatic burette glass is derived from Croatian-English Chemistry Dictionary & Glossary [28]

coprecipitation apparatus was developed in order to scale up the powder yield obtained from the coprecipitation process.

The semiautomatic coprecipitation apparatus consists of five main pieces of equipment, namely two magnetic stirrers, an electric pump, an apparatus controller, and an automatic burette. The schematic of the apparatus is shown in Fig. 1. The process starts with a magnetic stirrer, where iron sand was dissolved in an HCl solution for 60 minutes under a stirring speed of 1000 RPM. Subsequently, the electric pump automatically sent the yielded solution into the second magnetic stirrer for the titration process. Titration of NH_4OH into the yielded solution was carried out for 30 minutes under stirring at 1000 RPM. The apparatus controller automatically initiated the onset and operating time for both magnetic stirrers and the electric pump. The manual operation of the apparatus included the procedure of the automatic burette, namely pumping NH_4OH to the upper position of the burette, and opening and closing the burette valve. The final stage of coprecipitation comprises washing and drying the precipitates obtained in the second magnetic stirrer. The iron oxide powder obtained from the process was subjected to a gas nitriding process at 625°C in a tube furnace. The gas nitriding holding time was set at 2, 4, and 6 hours, with ammonia (NH_3) gas being applied at a flow rate of 150 mL/min.

Powder content was analyzed using XRD (Cu-Kα radiation, $\lambda = 1.54060$) with a PANalytical X'Pert Pro Diffractometer. Natural iron sand was also characterized through X-ray Fluorescence (XRF) analysis using a PANalytical MiniPal4. The magnetic properties of the samples were assessed with a Vibrating Sample Magnetometer (VSM) from the Physical Properties Measurement System Quantum Design PPMS® VersaLab™ Cryogen-free 3 Tesla. Lastly, the morphology of the powder samples was examined using Scanning Electron Microscopy (SEM) on a Zeiss EVO MA10.

3. Results and Discussion

3.1. Characterization of Natural Iron Sand

Before the coprecipitation process, raw natural iron sand was examined using XRF for component identification. Table 1 shows the result of the XRF measurement of iron sand. The natural iron sand consists mainly of Fe_3O_4 and several impurities such as Al_2O_3, SiO_2, and TiO_2. The composition is typical for Indonesian iron sand and has

Table 1. XRF result of as-received natural iron sand, indicating metal oxide content.

Phases	wt.%
Al_2O_3	0.90
SiO_2	0.90
P_2O_5	0.50
K_2O	0.10
CaO	0.28
TiO_2	12.30
V_2O_5	0.60
Cr_2O_3	0.04
MnO	0.50
Fe_3O_4	82.90
CuO	0.04
ZnO	0.80
Rb_2O	0.02
ZrO_2	0.02
Bi_2O_3	0.10

Table 2. Quantitative analysis result of iron sand.

Phase	Composition (wt.%)	Crystal Structure	Lattice Parameter (Å)	Sig
Fe_3O_4 (magnetite)	96.52	Cubic	$a = 8.4$	1.087
$FeTiO_3$ (ilmenite)	3.48	Trigonal	$a = 5.52$	1.087

been reported by numerous studies [13, 16, 29–32]. To improve the purity of Fe_3O_4, magnetic separation was performed on the iron sand. Subsequently, XRD examination was conducted, and the results are shown in Fig. 2.

Based on XRD analysis, iron sand consisted mainly of Fe_3O_4 (magnetite). A small peak of $FeTiO_3$ (ilmenite) was detected and could be regarded as an impurity. The phase identification was performed using Crystal Impact's Match! Software, based on COD IDs 1011085 for Fe_3O_4 and COD ID 9008036 for $FeTiO_3$. Additionally, quantitative analysis was carried out using MAUD software.

The result of the quantitative analysis is shown in Table 2. Fe_3O_4 is the majority phase with a content of 96.52%. Additional information such as the crystal structure and lattice parameters was determined. Based on XRD peak intensity and verification by quantitative analysis, $FeTiO_3$ has a small content of 3.47%. The presence of $FeTiO_3$ after magnetic separation is plausible, due to its weak magnetic nature. Therefore, some $FeTiO_3$ can still be present after separation. The formation of the hexagonal $FeTiO_3$ phase is attributed to the reaction between TiO_2 and FeO present in the sample [20].

3.2. Coprecipitation Result

Approximately two batches of the coprecipitation process were performed, each using 12 g of iron sand. In this study, two samples were obtained from each batch and labeled as Sample 1 and Sample 2. The coprecipitation process was carried out using the semiautomatic coprecipitation apparatus. Fig. 3 shows the XRD patterns of Sample 1 and Sample 2 obtained from the coprecipitation process. By comparing the XRD patterns with COD ID 9002320, it was determined that both samples comprise Fe_3O_4.

Crystallite size of both samples was determined using Scherrer's formula as shown in Eq. 1,

$$D = \frac{0.9\lambda}{\mathrm{FWHM}\cos\theta} \tag{1}$$

Based on the Scherrer formula, the crystal size of Fe_3O_4 in Sample 1 and Sample 2 is 39.22 nm and 37.61 nm, respectively. The difference in crystal size is influenced by pH, as reported by other studies [27, 33, 34]. However, the difference can be considered low, accounting for approximately 4.3%. This indicates that the coprecipitation process is capable of producing nano-scale iron oxide powder, which is beneficial for the synthesis of Fe_3N, providing more surface area for the nitridation process [35, 36].

The results on the iron oxide content and crystal size of both Samples 1 and 2 show that the semiautomatic coprecipitation apparatus can produce nanopowder from iron sand. The synthesis of Fe_3O_4 from natural iron sand, using the coprecipitation method, has been reported by many studies [15, 16, 27, 33, 37]. The formation of Fe_3O_4 during coprecipitation has also been deeply investigated, and the mechanism in reactions 2 to 5 is considered pro-

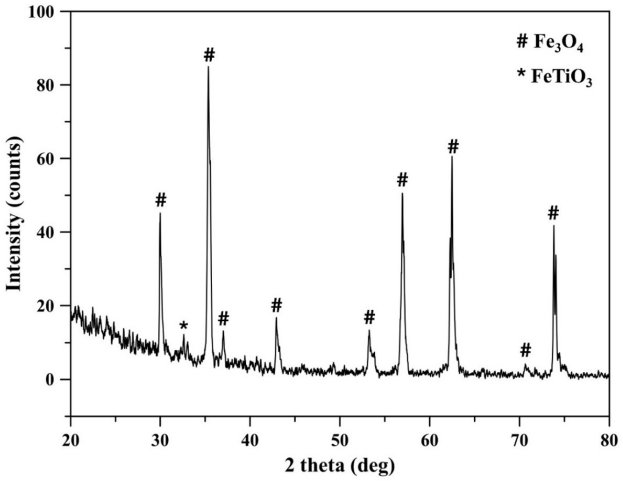

Figure 2. XRD pattern of natural iron sand as starting material

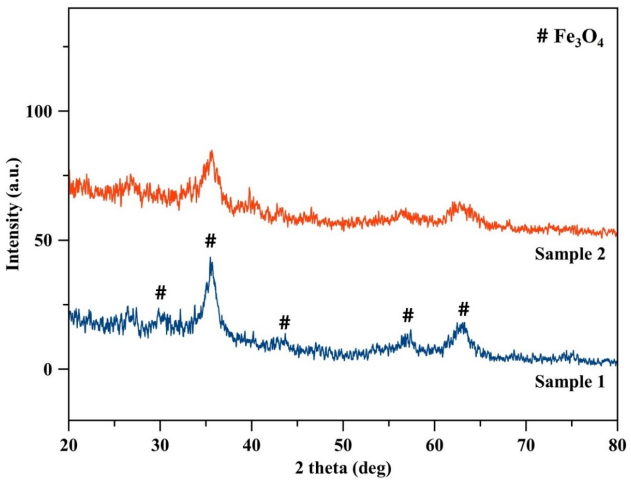

Figure 3. XRD pattern of Fe_3O_4 samples yielded from semiautomatic coprecipitation apparatus

Table 3. Fe_3O_4 yields using semiautomatic coprecipitation apparatus.

Name	Initial Weight (gr)	Final Weight (gr)	Yield (%)
Sample 1	12.0026	4.7278	39.38
Sample 2	12.0034	4.9859	41.53
	Average	$\mathbf{4.8569 \pm 0.18}$	$\mathbf{40.46 \pm 1.52}$

bable.

$$\mathrm{Fe}^{3+}(aq) + 3\mathrm{OH}^{-}(aq) \rightarrow \mathrm{Fe(OH)}_3(s) \quad (2)$$

$$\mathrm{Fe(OH)}_3(s) \rightarrow \mathrm{FeOOH}(s) + \mathrm{H_2O}(l) \quad (3)$$

$$\mathrm{Fe}^{2+}(aq) + 2\mathrm{OH}^{-}(aq) \rightarrow \mathrm{Fe(OH)}_2(s) \quad (4)$$

$$2\mathrm{FeOOH}(s) + \mathrm{Fe(OH)}_2(s) \rightarrow \mathrm{Fe_3O_4}(s) + 2\mathrm{H_2O}(l) \quad (5)$$

The Fe^{3+}(aq) or Fe^{2+}(aq) species are the products of dissolving iron sand in an HCl solution. Subsequently, titration of NH_4OH produces iron (II) hydroxide and iron (III) oxyhydroxide. Both species are considered to react during the titration process, forming magnetite nuclei as shown by Reaction 5.

Fig. 4 shows the SEM images of the iron oxide samples. The particle shape of both samples is typical, entailing chip-like particles. Additionally, the particle size is comparable, ranging from small chips to larger chip particles. Agglomeration of smaller particles is also observed in both samples, including the morphology of the magnetite particles, as reported by Duma et al. [16].

The semiautomatic coprecipitation apparatus used in the experiment can produce nano-sized Fe_3O_4 powder with consistent results. Table 3 shows the amount of Fe_3O_4 obtained by the apparatus. The initial weight represents the weight of the iron sand used in the coprecipitation, while the final weight shows the final product (Fe_3O_4) weight after the coprecipitation. Comparable results and similar yields were obtained from the two samples produced by the apparatus, showing the potential to produce consistent outcomes. Subsequently, the samples were used in the gas nitriding process to produce Fe_3N materials.

3.3. Gas Nitriding Result

Nitriding of Fe_3O_4 powder was carried out at 625°C under flowing NH_3 gas for different holding times, namely 2, 4, and 6 hours. Subsequently, some analyses were performed on the final product. Fig. 5 shows the XRD patterns of the powder after gas nitriding at different holding times. After 2 hours of nitriding, ε-Fe_3N was formed, while Fe_3N was detected after 4 and 6 hours. Other phases detected in the XRD patterns were iron oxides, Fe_3O_4, and Fe_2O_3 in the powder samples. The presence of both Fe_3O_4 and Fe_2O_3 showed that the parameters used during gas nitriding were not sufficient to form Fe_3N. Specifically, Fe_2O_3 was most likely formed due to oxidation, indicating that the nitriding parameters, namely flow and pressure, were not sufficient.

The efficiency of gas nitriding is primarily influenced by key process parameters, namely temperature, time, atmosphere pressure, and NH_3 flow rate. These parame-

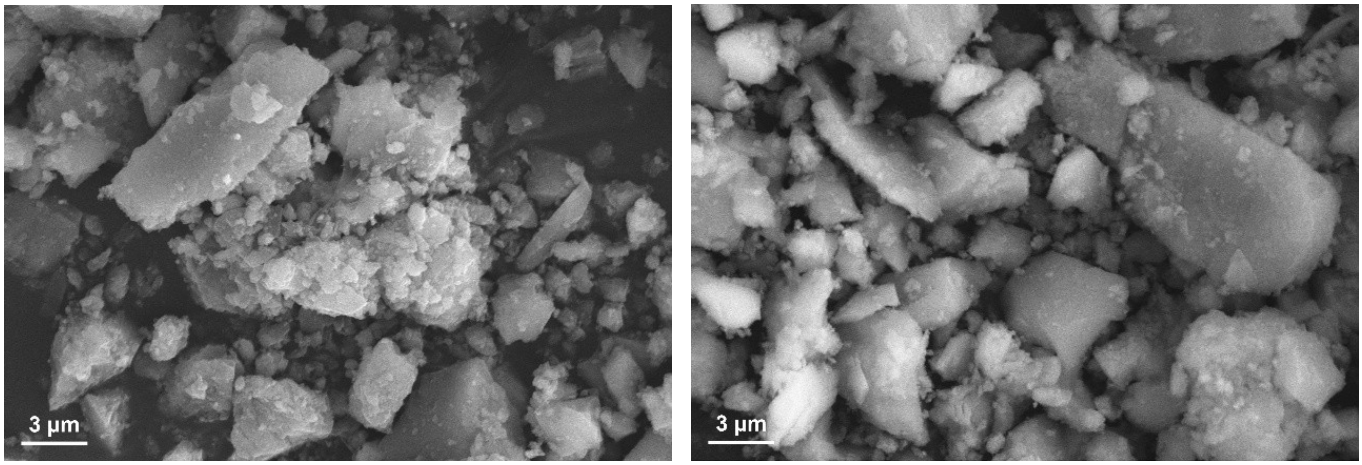

(a) **(b)**

Figure 4. SEM images of iron oxide samples. (a) Sample 1. (b) Sample 2

Table 4. Comparison of the number of phases formed in each variation using MAUD analysis.

Sample	Sig	Rwp (%)	Fe_2O_3 (wt.%)	Fe_3O_4 (wt.%)	Fe_3N (wt.%)
Nitriding time 2 hours	1.196697	36.58697	58.45	39.21	2.33
Nitriding time 4 hours	1.1798414	35.03525	68.99	19.94	11.06
Nitriding time 6 hours	1.140956	7.188651	53.85	11.94	34.19

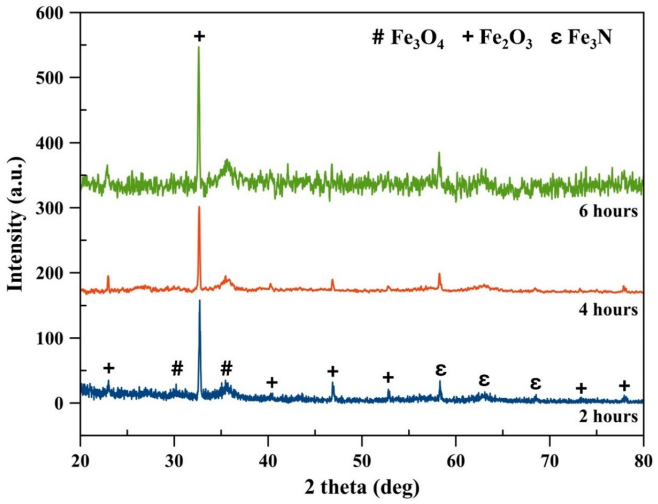

Figure 5. XRD patterns of powder sample after nitriding at different holding times

ters work together within the nitriding process [38]. The nitriding temperature used in this experiment can form Fe_3N, as suggested by other studies [5,39,40], which used a lower temperature. However, this experiment obtained a lower amount of Fe_3N, indicating ineffective control of other nitriding parameters such as gas mixing and gas purity.

The formation of Fe_3N during gas nitriding of iron oxide comprises a reduction process, which produces α-Fe and the final products [5,39,40]. The majority of studies on the synthesis of Fe_3N by gas nitriding combine NH_3 gas and H_2 gas, using Fe or Fe_2O_3 as the starting powder [2,5,41]. Therefore, the reduction of the powder is more assisted due to the presence of H_2 gas, obtaining single-phase Fe_3N.

Jovičević-Klug et al. reported that NH_3 gas produces a lower reduction degree than H_2 gas [39]. This suggests that a longer time is required to synthesize single-phase Fe_3N by gas nitriding of Fe_3O_4 powder with NH_3. Consequently, the presence of Fe_2O_3 and Fe_3O_4 is still detected in the sample with a nitriding time of 6 hours.

Table 4 shows the composition of phases formed after gas nitriding for different holding times. The composition is determined using quantitative analysis using MAUD software. The amount of Fe_3N increases with prolonged holding time due to an increase in nitrogen diffusion [42]. Subsequently, both iron oxides decrease, indicating that more Fe_3O_4 is transformed into Fe_3N.

Based on XRD analysis, the final powder consists predominantly of iron oxides. The highest amount of Fe_3N obtained in this experiment is 34.19 wt%. Therefore, the morphology of the final powder should be dominated by the iron oxide structure. As shown in Fig. 6 and Fig. 7, some powder still retains the shape of Fe_3O_4. This is because Fe_3N forms small particles on the surface of iron oxide particles as suggested by Ge et al. [2]. The higher magnification SEM image, depicted in Fig. 8, indicates small particles on the surface.

The particle is presumably Fe_3N because it has a similar irregular spherical-ellipsoidal shape. Smaller particles with a plate-like shape are also observed. The plate-like shape is attributed to Fe_3N, based on the report of other works [5,43]. Although Energy Dispersive Spectroscopy (EDS) can confirm the presence of Fe_3N particles, the XRD results collectively support the formation process. Moreover, future studies are recommended to include elemental mapping.

The magnetic properties of Fe_3N samples were studied by measuring the hysteresis loop using the VSM method, under room temperature. Fig. 9 shows the hysteresis loops of the Fe_3N material obtained after nitriding for different holding times. Magnetic properties, derived from the hysteresis loop, are shown in Table **??**. As the nitriding time was increased from 2 to 6 hours, the value of saturation magnetization reached 16.80, 16.41, and 17.21 emu/g, respectively. The magnetization values observed in all samples were lower than those reported in previous results [2,44–46]. This low value is due to the persistent presence of iron oxides, namely Fe_2O_3 and Fe_3O_4, acting as contaminants. Since the saturation magnetization values of the two phases are inherently smaller than that of Fe_3N [47], their presence directly contributes to the overall reduction in saturation magnetization, an effect also observed in the literature [4,48].

Although insignificant, a decrease in the saturation magnetization value is observed in the Fe_3N sample after nitriding for 4 hours. This decrease can be explained by the composition of phases in the sample, consisting of iron oxides. The results were unexpected since longer nitriding times should yield a higher amount of Fe_3N [38,49]. The condition can arise from the gas nitriding process during the experiment. Moreover, it is possible that leakage might have occurred in the area of the gas fittings during nitriding for 4 hours, which introduced more air into the tube furnace, leading to the oxidation of Fe_3O_4.

Other magnetic properties of Fe_3N samples are

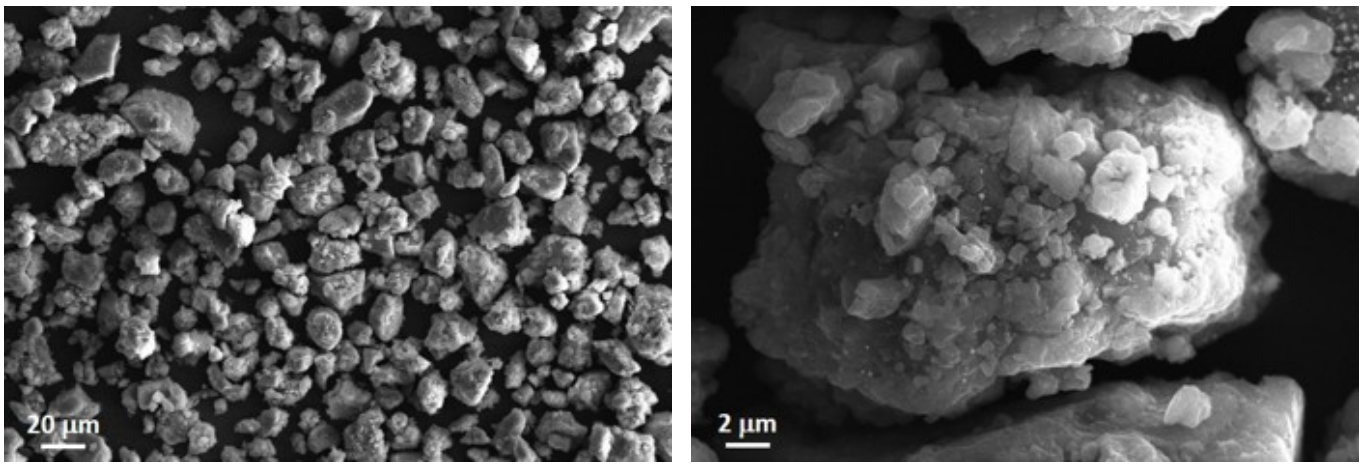

(a) (b)

Figure 6. SEM image showing the morphology of the powder sample after nitriding for 2 hours. (a) Magnification 1000X. (b) Magnification 10.000X.

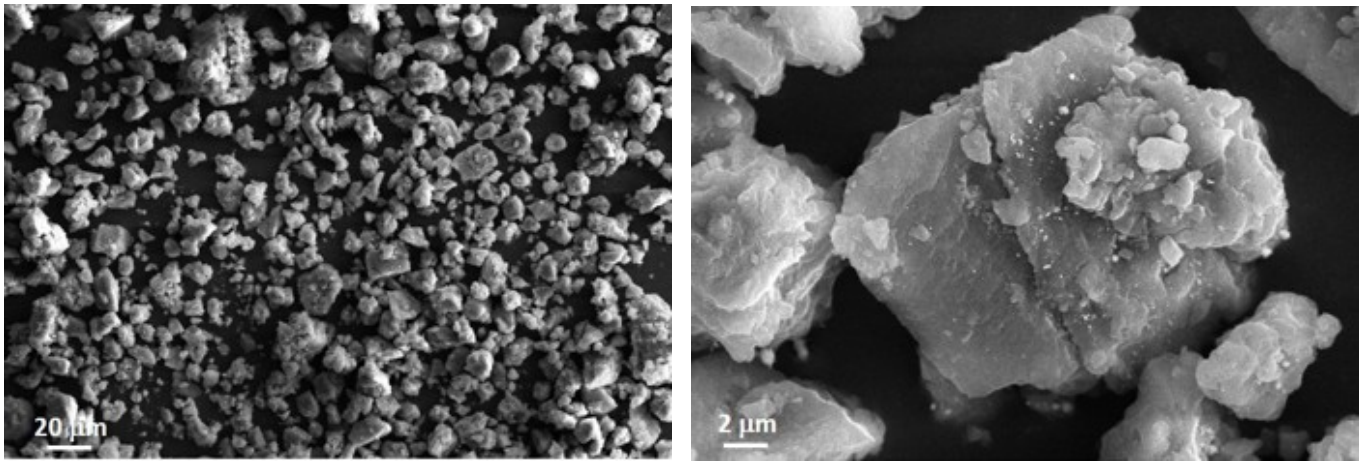

(a) (b)

Figure 7. SEM image showing the morphology of the powder sample after nitriding for 6 hours. (a) Magnification 1000X. (b) Magnification 10.000X.

shown in Table 5. The coercivity increases with longer nitriding time, reaching 21.58 Oe after 6 hours. The change in coercivity value can be associated with the formation of iron oxides, particularly Fe_2O_3. Fe_2O_3, most likely formed due to oxidation as described previously, may increase the coercivity of soft magnetic materials as reported by several works [50–52]. Therefore, there is a tendency for increasing coercivity with the increase in iron oxide content. This phenomenon occurs when the nitriding time is longer. The powder sample after 4 hours of nitriding showed the highest coercivity. The peculiar behavior indicated the same event, promoting the formation of more iron oxides, particularly as previously described. However, the coercivity value was small and could be considered typical of soft magnets. The retentivity increased with prolonged nitriding time.

Table 5. Magnetic properties of the final powder samples.

Sample	Saturation Magnetization (emu/g)	Retentivity (emu/g)	Coercivity (Oe)
Nitriding time 2 hours	16.80	0.028	3.16
Nitriding time 4 hours	16.41	0.211	26.72
Nitriding time 6 hours	17.21	0.309	21.58

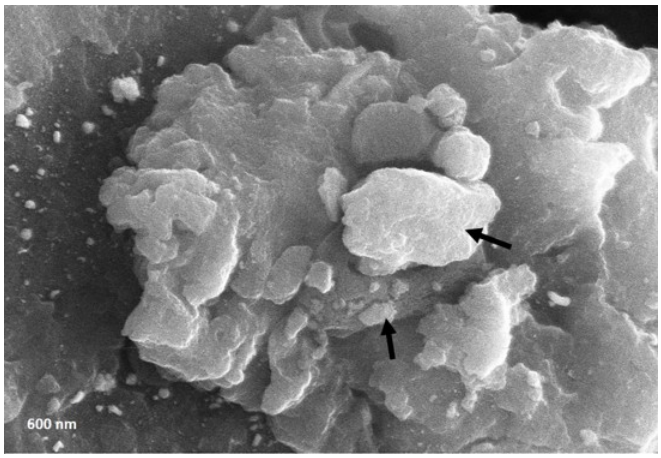

Figure 8. Higher magnification SEM image of the final powder after nitriding for 6 hours. Arrows indicate the iron nitride particle

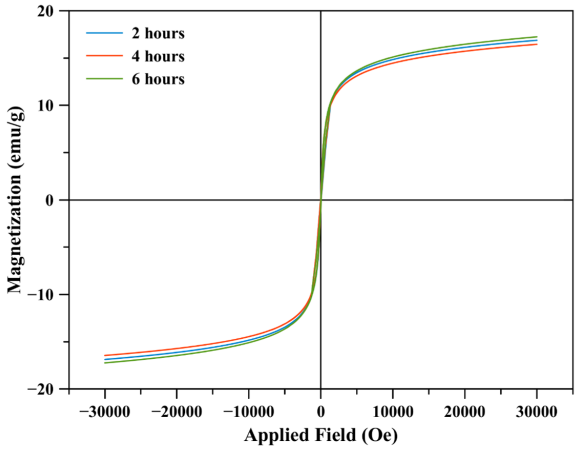

Figure 9. Hysteresis curves of the powder after nitriding at different durations

4. Conclusions

In conclusion, the semiautomatic coprecipitation apparatus was implemented in the synthesis of Fe_3N, using natural iron sand as the raw material. The apparatus successfully produced consistent Fe_3O_4 yields, as shown by the XRD and SEM results. The Fe_3O_4 samples obtained had typical crystallite size and morphology. Subsequently, the Fe_3O_4 samples were used as the starter material in gas nitriding. After gas nitriding at different holding times, Fe_3N was obtained, as indicated by the XRD results. Iron oxides, Fe_3O_4 and Fe_2O_3, were also detected, indicating that the nitriding parameters used were insufficient to produce single-phase Fe_3N. The magnetic properties of the final product showed characteristics typical of a soft magnet material. The maximum value of saturation magnetization was obtained after nitriding for 6 hours. This work provides a promising pathway toward utilizing Indonesia's natural resources for soft magnetic material production.

References

[1] X. Tan, S. Wang, Y. Chen, Y. Zhou, and Z. Li, "Design, preparation and characterization of iron nitride magnetic abrasives," *Journal of Alloys and Compounds*, vol. 774, pp. 443–450, feb 2019.

[2] M. Ge *et al.*, "Effects of gas nitridation on microstructures and magnetic properties of fe$_3$n/fe soft magnetic composites," *Journal of Materials Science: Materials in Electronics*, vol. 33, pp. 10287–10296, may 2022.

[3] M. Gong, P. Li, and W. Tong, "Absorption properties of iron nitrides particles fabricated by ball milling," in *AIP Conference Proceedings*, vol. 1995, p. 030021, jul 2018.

[4] J. Kim, J. Hwang, and S. Yi, "Iron nitride based magnetic powder synthesized by mechanical alloying of fe-based glassy powders and solid nitrogen compounds," *Journal of Magnetism and Magnetic Materials*, vol. 539, p. 168329, dec 2021.

[5] K. Wu *et al.*, "Irregularly shaped iron nitride nanoparticles as a potential candidate for biomedical applications: From synthesis to characterization," *ACS Omega*, vol. 5, pp. 11756–11767, may 2020.

[6] S. Bhattacharyya, "Iron nitride family at reduced dimensions: A review of their synthesis protocols and structural and magnetic properties," *The Journal of Physical Chemistry C*, vol. 119, pp. 1601–1622, jan 2015.

[7] J. Lei *et al.*, "Effects of heat treatment and lubricant on magnetic properties of iron-based soft magnetic composites with al$_2$o$_3$ insulating layer by one-pot synthesis method," *Journal of Magnetism and Magnetic Materials*, vol. 472, pp. 7–13, feb 2019.

[8] Z. Birčáková *et al.*, "Magnetic properties of fe-based soft magnetic composite with insulation coating by resin bonded ni–zn ferrite nanofibres," *Journal of Magnetism and Magnetic Materials*, vol. 485, pp. 1–7, sep 2019.

[9] Á. S. Muñoz *et al.*, "Study of an iron phosphate soft magnetic composite and its stability at high temperatures," *Ceramics International*, vol. 50, pp. 22468–22478, jul 2024.

[10] H. Sun *et al.*, "Magnetic properties of iron-based soft magnetic composites prepared by utilizing polyimide insulating layer," *Journal of Magnetism and Magnetic Materials*, vol. 486, p. 165287, sep 2019.

[11] I. Sidharta, R. F. Syah, S. Sutikno, D. Darminto, and A. Shahab, "Exploring the potential of indonesian iron sand in the formation of iron nitride for magnetic applications," *Mechanical Engineering for Society and Industry*, vol. 5, pp. 257–267, jun 2025.

[12] M. R. Fahlepy, V. A. Tiwow, and Subaer, "Characterization of magnetite (fe_3o_4) minerals from natural iron sand of bonto kanang village takalar for ink powder (toner) application," in *Journal of Physics: Conference Series*, vol. 997, p. 012036, mar 2018.

[13] Y. E. Gunanto, M. P. Izaak, E. Jobiliong, L. Cahyadi, and W. A. Adi, "High purity fe_3o_4 from local iron sand extraction," in *Journal of Physics: Conference Series*, vol. 1011, p. 012005, apr 2018.

[14] R. Rahmawati *et al.*, "Synthesis of magnetite (fe_3o_4) nanoparticles from iron sands by coprecipitation-ultrasonic irradiation methods," *Journal of Materials and Environmental Sciences*, vol. 9, no. 1, pp. 155–160, 2018.

[15] S. T. Wicaksono, A. Wahfiudin, A. D. Pramata, and S. Sagadevan, "Effect of fe (iii)/fe (ii) cation molar ratio variation on magnetite fe_3o_4 nanoparticles synthesized from natural iron sand by co-precipitation method," *MRS Advances*, vol. 9, pp. 1593–1597, dec 2024.

[16] T. N. Duma *et al.*, "Study of crystal structure, lattice strain, and elemental content of natural iron sand nanoparticles synthesized by the coprecipitation method," *Environment and Natural Resources Journal*, vol. 23, jan 2025.

[17] F. Hartono, P. Widiyanti, and A. H. Zaidan, "Iron sand-based and ionic-based magnetic nanoparticle physical characteristics comparison for biomedical application," in *AIP Conference Proceedings*, vol. 2536, p. 050002, may 2023.

[18] S. N. Qoidah *et al.*, "Fe_3o_4/mwcnt/tio_2 nanocomposites as excellent microwave absorber material," *Journal of Alloys and Compounds*, vol. 970, p. 172590, jan 2024.

[19] A. Taufiq *et al.*, "Synthesis of fe_3o_4/ag nanohybrid ferrofluids and their applications as antimicrobial and antifibrotic agents," *Heliyon*, vol. 6, p. e05813, dec 2020.

[20] R. Ramlan, A. A. Bama, A. Johan, M. Naibaho, and M. Ginting, "Synthesis and characterization of hematite (α-fe_2o_3) from iron sand using coprecipitation method," in *Key Engineering Materials*, vol. 985, pp. 145–151, 2024.

[21] A. Ali *et al.*, "Synthesis, characterization, applications, and challenges of iron oxide nanoparticles," *International Journal of Nanomedicine*, vol. 11, pp. 49–67, aug 2016.

[22] N. Novita, R. Ramlan, M. Naibaho, M. Ginting, S. Humaidi, and T. N. Duma, "Fe_2o_3 review: Nanostructure, synthesis methods, and applications," *International Journal of Social Service and Research*, vol. 4, pp. 539–559, feb 2024.

[23] M. T. Spicher *et al.*, "Pilot-scale co-precipitation synthesis of a novel active ingredient made of ultrasmall iron (oxyhydr)oxide nanoparticles for the treatment of hyperphosphatemia," *RSC Advances*, vol. 14, pp. 16117–16127, may 2024.

[24] R. Zauner and A. G. Jones, "Scale-up of continuous and semibatch precipitation processes," *Industrial & Engineering Chemistry Research*, vol. 39, pp. 2392–2403, jul 2000.

[25] M. P. Moreira and D. Grasseschi, "Automation of a low-cost device for flow synthesis of iron oxide nanoparticles," *Journal of Nanoparticle Research*, vol. 24, p. 93, apr 2022.

[26] C.-C. Lin, Y.-P. Lai, and K.-Y. Wu, "A high-productivity process for mass-producing fe_3o_4 nanoparticles by co-precipitation in a rotating packed bed," *Powder Technology*, vol. 395, pp. 369–376, jan 2022.

[27] Sunaryono *et al.*, "Various magnetic properties of magnetite nanoparticles synthesized from iron-sands by coprecipitation method at room temperature," in *Materials Science Forum*, vol. 827, pp. 229–234, 2015.

[28] E. Generalic, "Automatic burette." Croatian-English Chemistry Dictionary & Glossary, 2025. Accessed: Jun. 12, 2025.

[29] N. R. Ardiani, S. Setianto, B. Santosa, B. M. Wibawa, C. Panatarani, and I. M. Joni, "Quantitative analysis of iron sand mineral content from the south coast of cidaun, west java using rietveld refinement method," in *AIP Conference Proceedings*, vol. 2219, p. 040003, may 2020.

[30] Fahmiati, Nuryono, and Suyanta, "Characteristics of iron sand magnetic material from bugel beach, kulon progo, yogyakarta," in *IOP Conference Series: Materials Science and Engineering*, vol. 172, p. 012020, feb 2017.

[31] Maulinda, I. Zein, and Z. Jalil, "Identification of magnetite material (fe_3o_4) based on natural materials as catalyst for industrial raw material application," in *Journal of Physics: Conference Series*, vol. 1232, p. 012054, sep 2019.

[32] Y. E. Gunanto, M. P. Izaak, L. Cahyadi, E. Jobiliong, and W. A. Adi, "Preliminary study: Local iron sand characterization of titanomagnetite type," in *IOP Conference Series: Materials Science and Engineering*, vol. 367, p. 012059, may 2018.

[33] N. P. D. Kristina, I. G. Arjana, and P. Yasa, "Synthesis and characterization of magnetite nanomaterials in tianyar iron sand using co-precipitation method," *Indonesian Physical Review*, vol. 7, pp. 398–413, jul 2024.

[34] B. H. Hui and M. N. Salimi, "Production of iron oxide nanoparticles by co-precipitation method with optimization studies of processing temperature, ph and stirring rate," in *IOP Conference Series: Materials Science and Engineering*, vol. 743, p. 012036, feb 2020.

[35] S. H. Kayani, H. M. S. Ajmal, B.-J. Kim, N.-K. Park, and K. Euh, "Influence of powder size on pore characteristics and intermetallic phase kinetics in porous ti-al alloys," *Crystals*, vol. 14, p. 559, jun 2024.

[36] A. Albrecht and D. Moszyński, "Nitriding and denitriding of nanocrystalline iron system with bimodal crystallite size distribution," *Materials*, vol. 15, p. 143, jan 2022.

[37] C. Wroblewski, T. Volford, B. Martos, J. Samoluk, and P. Martos, "High yield synthesis and application of magnetite nanoparticles (fe_3o_4)," *Magnetochemistry*, vol. 6, p. 22, jun 2020.

[38] Y.-L. Zhou, F. Xia, A.-J. Xie, H.-P. Peng, J.-H. Wang, and Z.-W. Li, "A review—effect of accelerating methods on gas nitriding: Accelerating mechanism, nitriding behavior, and techno-economic analysis," *Coatings*, vol. 13, p. 1846, nov 2023.

[39] M. Jovičević-Klug, Y. Ma, P. Jovičević-Klug, J. M. Prabhakar, M. Rohwerder, and D. Raabe, "Thermal kinetics and nitriding effect of ammonia-based direct reduction of iron oxides," *ACS Sustainable Chemistry & Engineering*, vol. 12, pp. 9882–9896, jul 2024.

[40] W. Arabczyk, R. Pelka, I. Kocemba, A. Brzoza-Kos, A. Wyszkowski, and Z. Lendzion-Bieluń, "Study of phase transformation processes occurring in the nanocrystalline iron/ammonia/hydrogen system by the magnetic permeability measurement method," *The Journal of Physical Chemistry C*, vol. 126, pp. 7704–7710, may 2022.

[41] C. Zhang *et al.*, "Preparation and soft magnetic properties of γ'-fe_4n particles," *Journal of Materials Science: Materials in Electronics*, vol. 29, jan 2018.

[42] N. E. Dan, S. N. S. M. Sabri, P. Hussain, and H. Mohebbi, "The influence of nitrogen on the wear resistance of ferritic stainless steel," in *Journal of Physics: Conference Series*, vol. 1082, p. 012109, aug 2018.

[43] J. Theerthagiri, S. B. Dalavi, M. M. Raja, and R. N. Panda, "Magnetic properties of nanocrystalline ε-fe_3n and co_4n phases synthesized by newer precursor route," *Materials Research Bulletin*, vol. 48, pp. 4444–4448, nov 2013.

[44] C. Zhang *et al.*, "Design, preparation, and magnetic properties of fe_4n/fe_3n soft magnetic composites fabricated by gas nitridation," *Journal of Superconductivity and Novel Magnetism*, feb 2023.

[45] W. Yin *et al.*, "Soft magnetic ε-fe_3n: Synthesis, characterization and magnetic properties," *Journal of Alloys and Compounds*, vol. 688, pp. 828–832, dec 2016.

[46] A.-M. Zieschang *et al.*, "Nanoscale iron nitride, ε-fe_3n: Preparation from liquid ammonia and magnetic properties," *Chemistry of Materials*, vol. 29, pp. 499–505, jan 2017.

[47] Y. Utsushikawa and K. Niizuma, "The saturation magnetization of fe-n films prepared by nitriding treatment in n_2 plasma," *Journal of Alloys and Compounds*, vol. 222, pp. 188–192, may 1995.

[48] V. Zhandun and A. Matsynin, "The effect of the impurities on the magnetic, electronic and optical properties of mn_5ge_3," *Chinese Journal of Physics*, vol. 68, pp. 9–18, dec 2020.

[49] P. Hussain, H. Mahmoud, S. N. Basha, and A. I. Mohamad, "Correlation between microstructure and micro-hardness of 316l nitrided austenitic stainless steel," in *IOP Conference Series: Materials Science and Engineering*, vol. 863, p. 012025, may 2020.

[50] G. Zhao, C. Wu, and M. Yan, "Fabrication and growth mechanism of iron oxide insulation matrix for fe soft magnetic composites with high permeability and low core loss," *Journal of Alloys and Compounds*, vol. 710, pp. 138–143, jul 2017.

[51] R. Khabirov *et al.*, "Mn–zn ferrites with high fe_2o_3 content obtained by the nitrate–citrate sol–gel autocombustion method," *International Journal of Applied Ceramic Technology*, vol. 22, p. e15193, sep 2025.

[52] M. Krajewski *et al.*, "Impact of thermal oxidation on chemical composition and magnetic properties of iron nanoparticles," *Journal of Magnetism and Magnetic Materials*, vol. 458, pp. 346–354, jul 2018.